Supporting Information

Engineered hole-free, spacer-free dye-sensitized light harvesters for indoor photovoltaic and self-powered applications

Andrew Simon George,[a,b] Sourava Chandra Pradhan,[a,b] K. N. Narayanan Unni [a,b] and Suraj Soman[a,b]*

[a] Centre for Sustainable Energy Technologies (C-SET), CSIR-National Institute for Interdisciplinary Science and Technology (CSIR-NIIST), Thiruvananthapuram 695019, India
[b] Academy of Scientific and Innovative Research (AcSIR), Ghaziabad, 201002, India
E-mail: suraj@niist.res.in

Supporting information includes:
Device fabrication & characterization
Figures S1 to S18
Tables S1 to S27
Schemes S1 and S2
References

Other Supplementary Material for this manuscript includes:
Supplementary video S1

Device fabrication & characterization

FTO substrates (TEC 15 Ω/cm^2, Greatcell Solar) used as photoanodes were sequentially cleaned in soap solution (Extran), distilled water, acetone, and isopropanol before being annealed at 500 °C using the programmed ramp heating of 325 °C for 15 min, 375 °C for 15 min, 450 °C for 15 min, and 500 °C for 30 min. This was followed by UV-Ozone treatment before pre-blocking layer deposition (immersed in 53 mM $TiCl_4$ solution for 30 min at a constant temperature of 70 °C followed by annealing at 500 °C). One layer of transparent mesoporous TiO_2 layer (18-NRT, Greatcell Solar) followed by a scattering layer (18-NR AO, Greatcell Solar) was screen printed using our home-built setup (Screen Printer, Elixir Technologies) resulting in an effective layer thickness of 6 µm and then annealed at 500°C using the same program as mentioned earlier. The post-blocking layer was deposited by immersing the TiO_2 coated electrodes in aqueous 40 mM $TiCl_4$ solution for 30 min at 70 °C followed by heat-treatment at 500 °C. The electrodes were then immersed in the prepared dye solution (XY1b (0.1 mM)) for the initial batch and D35:XY1b (1:1 ratio with 0.1 mM concentration of each dye in equal volume of acetonitrile and tert-butanol) co-sensitized combination for the later batches and kept at room temperature for 15 h for effective dye loading (dyes were procured from Dyenamo AB, Sweden). Counter electrodes (CE) (TEC 7 Ω/cm^2, Greatcell Solar) for the normal architecture devices were hole drilled (diameter of 0.7mm) before cleaning while for the HF-SF architecture, the CE were directly cleaned by following the same protocol used for the photoanode. Further, PEDOT deposition was done using Autolab-PGSTAT 302N (Metrohm) electrochemical workstation. The electrodes for the normal architecture were assembled as shown in Scheme 1(a). Here, the UV-curable epoxy resin (3035 B/ThreeBond) is deposited along the boundaries of the active area in the photoanode which facilitates as an effective spacer between the two electrodes. The PEDOT deposited CE is carefully aligned on top followed by UV irradiation for 5 minutes for effective epoxy curing. Electrolyte preparation for both $[Cu^{(I/II)}(dmp)_2]$ and $[Cu^{(I/II)}(dmby)_2]$ were done using standard concentrations [0.2M Cu(I) species, 0.04M Cu(II) species, 0.6M TBP and 0.1 M LiTFSI in acetonitrile] (copper electrolyte received from Dyenamo AB, Sweden). Further, electrolyte filling was done via electrolyte injection through the pre-drilled holes on the CE, followed by back sealing using cover glass for the normal device. In the case of HF-SF devices, as shown in Scheme 1(b), the assembling is done by directly sandwiching the electrodes with external force using a homemade assembling set-up followed by filling the electrolyte through the edges of electrodes. Further, the epoxy resin was deposited along the edges and UV cured to complete the fabrication.

J−*V* measurements under indoor light illumination was carried out using the standard Osram warm white (WW) CFL and WW LED bulbs in our custom-made black box arrangement (Figure S1) and the measurements were done using certified low power measuring unit from Dyenamo AB as detailed in our previous works.[1–4] The spectra of the indoor CFL and LED light sources at various illumination intensities along with their integrated power density curves are provided in Figure S2. The electrochemical impedance spectroscopy (EIS) in dark and

charge extraction measurements were performed using the Autolab-PGSTAT 302N (Metrohm) electrochemical workstation. For DSCs, three semicircles are mainly observed in the Nyquist plot. The semicircle in the high frequency region corresponds to the charge transfer at counter electrode/electrolyte interface, the second semicircle in the middle frequency region corresponds to charge transfer at TiO_2/dye/electrolyte interface and the third semicircle in the lower frequency region corresponds to the diffusion of ions in the electrolyte. Hence to explore the effect of HF-SF architecture at the interfaces, EIS measurement was carried out at an applied forward bias of 0.9 V, with a perturbation of amplitude 10 mV and frequency increasing logarithmically from 0.1 Hz to 100 kHz. Similarly, charge extraction is a light perturbation technique used to measure electron concentration at the TiO_2 network, which further provides information on the density of states and shift in conduction band of TiO_2. For charge extraction measurement, devices kept at open circuit condition is illuminated for a few seconds and the illumination is stopped while simultaneously short-circuiting the devices to extract the charge. Light perturbation techniques (transient photovoltage decay and transient photocurrent decay) was carried out using Toolbox (Dyenamo AB) to obtain the lifetime and transport time information on the fabricated DSCs. For transient photovoltage decay, solar cell is first open circuited and continuously illuminated till it reaches to a steady state V_{oc}. A square wave light perturbation is then superimposed with the steady state illumination and the voltage response of the solar cell is monitored. For transient photocurrent decay, the solar cell is short circuited and continuously illuminated till it reaches to the steady state J_{sc}. A square wave light perturbation is then superimposed with the steady illumination and the current response of the solar cell is further monitored.

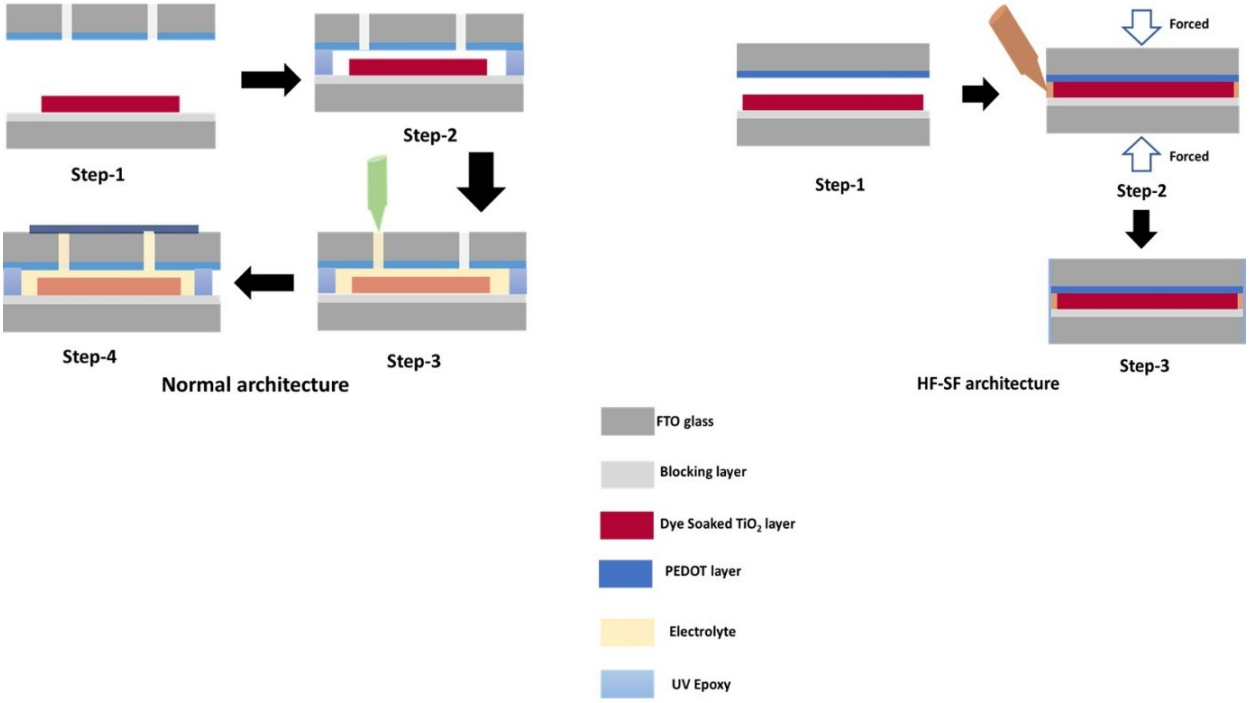

Scheme S1. Schematic representation of various device fabrication steps involved in the fabrication of DSCs with **(a)** Normal architecture, **(b)** HF-SF architecture.

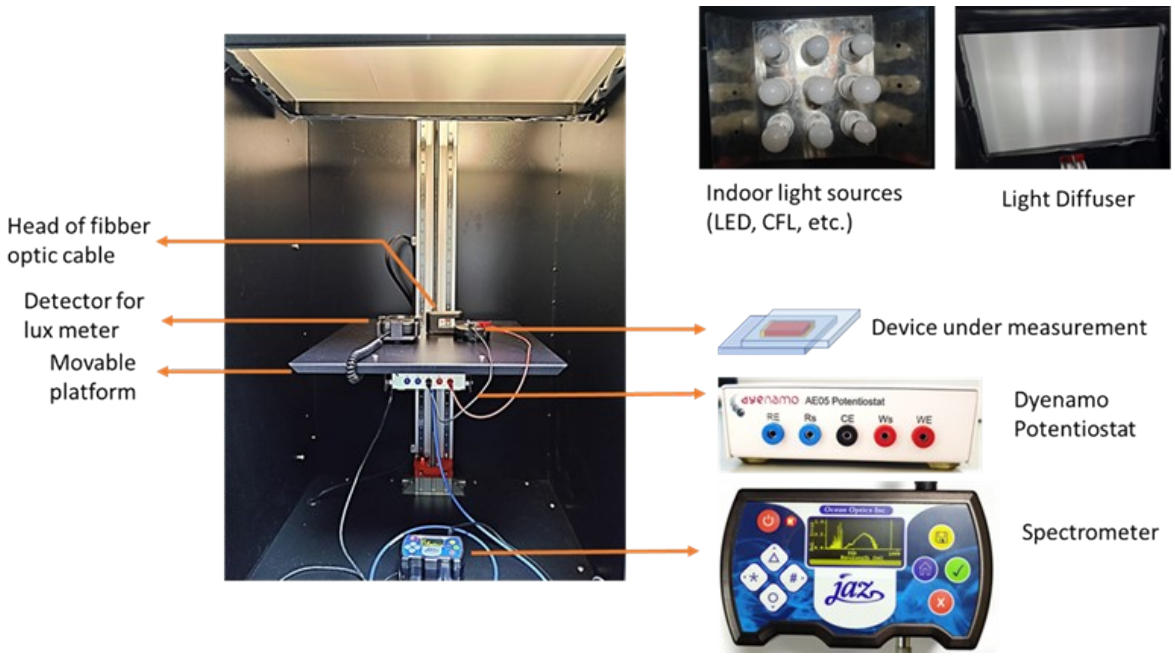

Figure S1. Custom-made black box arrangement for indoor *J-V* measurements.

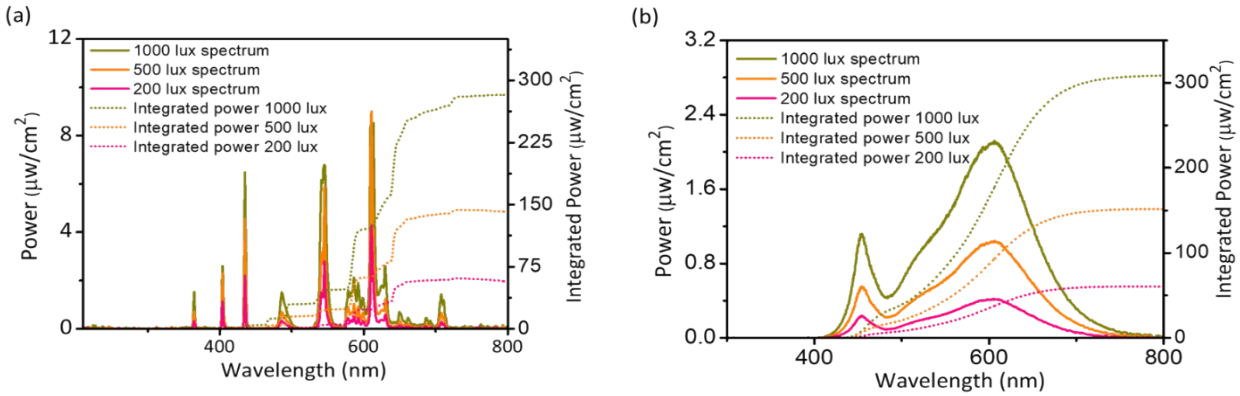

Figure S2. Emitted power density spectrum and integrated power density for **(a)** WW CFL and **(b)** WW LED light sources at various illumination intensities.

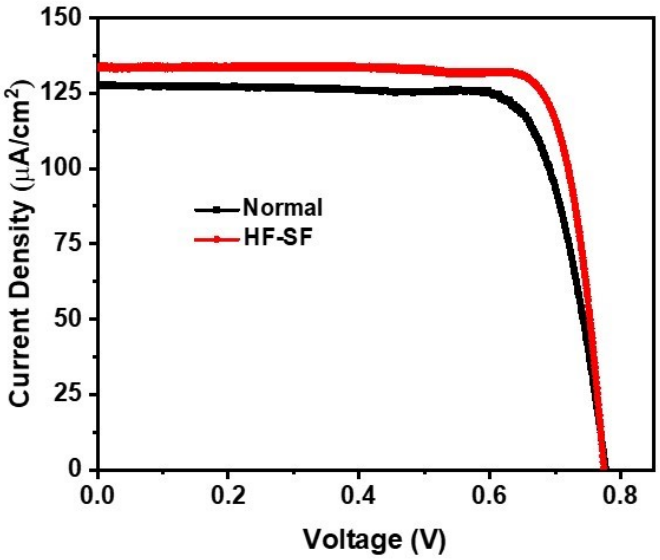

Figure S3. *J-V* graph under 1000 lux WW CFL illumination for normal and HF-SF DSCs using XY1b dye and $[Cu^{(I/II)}(dmp)_2]$ electrolyte.

Table S1. *J-V* data under 1000 lux WW CFL illumination for normal and HF-SF DSCs using XY1b dye and $[Cu^{(I/II)}(dmp)_2]$ electrolyte.

Device	V_{oc} **(V)**	J_{SC} **(μA/cm²)**	***FF***	***Efficiency*** **(%)**
Normal	0.77 ± 0.006	127.8 ± 0.65	78 ± 0.6	27.34 ± 0.26
HF-SF	0.75 ± 0.01	137.8 ± 4.99	82.9 ± 1.5	30.48 ± 0.23

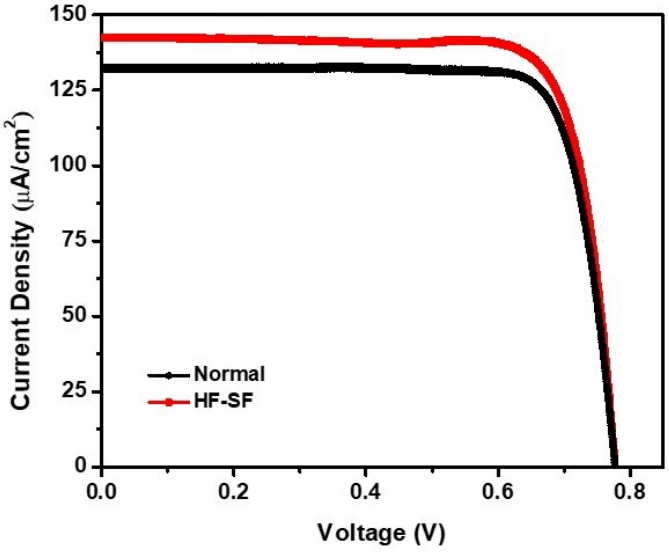

Figure S4. *J-V* graph under 1000 lux WW CFL illumination for normal and HF-SF DSCs using D35:XY1b co-sensitized dye and $[Cu^{(I/II)}(dmp)_2]$ electrolyte.

Table S2. *J-V* data under 1000 lux WW CFL illumination for normal and HF-SF DSCs using D35:XY1b co-sensitized dye and $[Cu^{(I/II)}(dmp)_2]$ electrolyte.

Device	V_{oc} (V)	J_{SC} (µA/cm²)	*FF*	*Efficiency* (%)
Normal	0.77 ± 0.002	133.6 ± 0.67	80.9 ± 4.77	29.51± 0.82
HF-SF	0.78 ± 0.025	142 ± 2.18	80.1 ± 2.37	31.33 ± 0.62

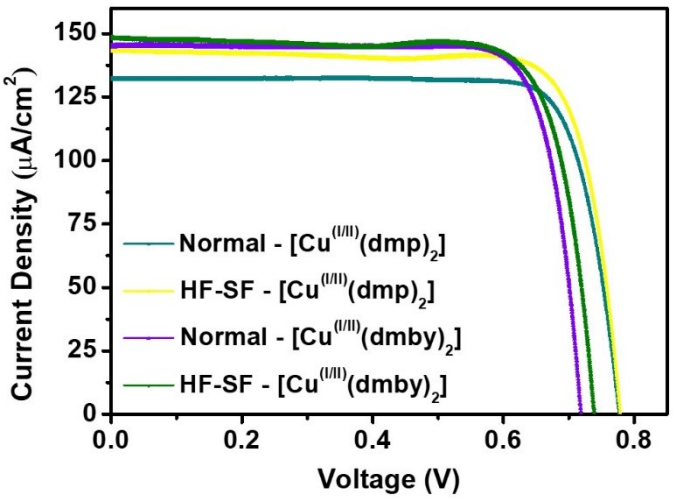

Figure S5. *J-V* graph for normal and HF-SF DSCs devices using D35:XY1b co-sensitized dye with $[Cu^{(I/II)}(dmp)_2]$ and $[Cu^{(I/II)}(dmby)_2]$ electrolytes under 1000 lux WW CFL illumination.

Table S3. *J-V* data for normal and HF-SF DSCs using D35:XY1b co-sensitized dye with $[Cu^{(I/II)}(dmp)_2]$ and $[Cu^{(I/II)}(dmby)_2]$ electrolytes under 1000 lux WW CFL illumination.

Device	Electrolyte	V_{OC} (V)	J_{SC} (µA/cm²)	*FF*	*Efficiency* (%)
Normal	$[Cu^{(I/II)}(dmp)_2]$	0.77 ± 0.002	133.6 ± 0.67	80.9 ± 4.77	29.51± 0.82
HF-SF		0.78 ± 0.025	142 ± 2.18	80.1 ± 2.37	31.33 ± 0.62
Normal	$[Cu^{(I/II)}(dmby)_2]$	0.72 ± 0.010	144.8 ± 1.42	81.6 ± 0.60	30.01 ± 0.22

HF-SF	0.74 ± 0.007	148.4 ± 0.98	78.5 ± 1.97	30.40 ± 0.22

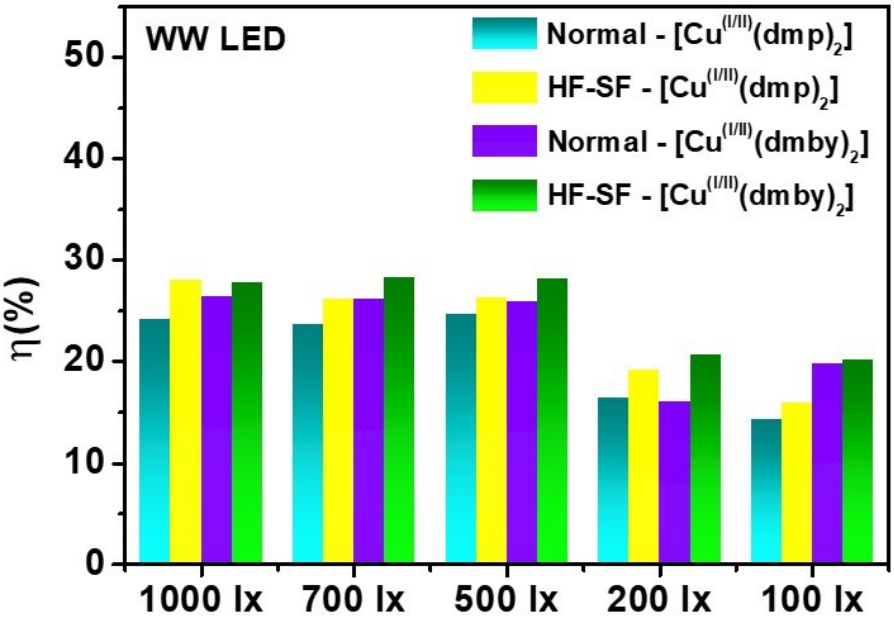

Figure S6. Efficiency as a function of illumination intensity for normal and HF-SF DSCs under WW LED illumination (1000 – 100 lux) employing $[Cu^{(I/II)}(dmp)_2]$ and $[Cu^{(I/II)}(dmby)_2]$ electrolyte using co-sensitized D35:XY1b dye.

Table S4. *J-V* data for normal and HF-SF DSCs using D35:XY1b co-sensitized dye and $[Cu^{(I/II)}(dmp)_2]$ and $[Cu^{(I/II)}(dmby)_2]$ electrolytes under 700 lux WW CFL illumination (P_{in} – 195.45 μW/cm^2).

DEVICE	ELECTROLYTE	V_{OC} (V)	J_{SC} (MA/CM^2)	*FF*	EFFICIENCY (%)
Normal		0.73	95.8	80.1	28.58
HF-SF	$[Cu^{(I/II)}(dmp)_2]$	0.76	98.9	80.1	30.90
Normal		0.73	92.2	81.4	28.01
HF-SF	$[Cu^{(I/II)}(dmby)_2]$	0.72	100.4	79.8	29.75

Table S5. *J-V* data for normal and HF-SF DSCs using D35:XY1b co-sensitized dye with $[Cu^{(I/II)}(dmp)_2]$ and $[Cu^{(I/II)}(dmby)_2]$ electrolytes under 500 lux WW CFL illumination (P_{in} – 143.05 μW/cm^2).

DEVICE	ELECTROLYTE	V_{OC} (V)	J_{SC} (MA/CM^2)	*FF*	EFFICIENCY (%)
Normal		0.75	65.9	80.2	27.78
HF-SF	$[Cu^{(I/II)}(dmp)_2]$	0.75	73.8	80.6	31.16
Normal		0.71	71.9	81.1	29.16
HF-SF	$[Cu^{(I/II)}(dmby)_2]$	0.72	75.2	79.2	30.24

Table S6. *J-V* data for normal and HF-SF DSCs using D35:XY1b co-sensitized dye with $[Cu^{(I/II)}(dmp)_2]$ and $[Cu^{(I/II)}(dmby)_2]$ electrolytes under 200 lux WW CFL illumination (P_{in} – 59.11 μW/cm^2).

DEVICE	ELECTROLYTE	V_{OC} (V)	J_{SC} (MA/CM^2)	*FF*	EFFICIENCY (%)
Normal		0.71	24	79.7	23.32
HF-SF	$[Cu^{(I/II)}(dmp)_2]$	0.71	26	75.3	24.83
Normal		0.67	24.7	81.2	22.94
HF-SF	$[Cu^{(I/II)}(dmby)_2]$	0.68	26.5	85.9	26.30

Table S7. *J-V* data for normal and HF-SF DSCs using D35:XY1b co-sensitized dye with $[Cu^{(I/II)}(dmp)_2]$ and $[Cu^{(I/II)}(dmby)_2]$ electrolytes under 100 lux WW CFL illumination (P_{in} – 28.47 μW/cm^2).

DEVICE	ELECTROLYTE	V_{OC} (V)	J_{SC} (MA/CM^2)	*FF*	EFFICIENCY (%)
Normal		0.67	10.7	73.7	18.86
HF-SF	$[Cu^{(I/II)}(dmp)_2]$	0.67	13.5	75.3	24.25
Normal		0.65	12.54	79.2	22.71
HF-SF	$[Cu^{(I/II)}(dmby)_2]$	0.66	12.56	85.1	24.77

Table S8. *J-V* data for normal and HF-SF DSCs using D35:XY1b co-sensitized dye with $[Cu^{(I/II)}(dmp)_2]$ and $[Cu^{(I/II)}(dmby)_2]$ electrolytes under 1000 lux WW LED illumination (P_{in} – 303.16 μW/cm^2).

DEVICE	ELECTROLYTE	V_{OC} (V)	J_{SC} (MA/CM^2)	*FF*	EFFICIENCY (%)
Normal		0.77	121	78	24.17
HF-SF	$[Cu^{(I/II)}(dmp)_2]$	0.77	138.2	79.5	28.07
Normal		0.74	140.1	77.3	26.42
HF-SF	$[Cu^{(I/II)}(dmby)_2]$	0.74	143.3	79.4	27.8

Table S9. *J-V* data for normal and HF-SF DSCs using D35:XY1b co-sensitized dye with $[Cu^{(I/II)}(dmp)_2]$ and $[Cu^{(I/II)}(dmby)_2]$ electrolytes under 700 lux WW LED illumination (P_{in} – 208.94 μW/cm^2).

DEVICE	ELECTROLYTE	V_{OC} (V)	J_{SC} (MA/CM^2)	*FF*	EFFICIENCY (%)
Normal		0.76	84.8	76.3	23.65
HF-SF	$[Cu^{(I/II)}(dmp)_2]$	0.76	89.6	80.1	26.09
Normal		0.73	95	78.4	26.19
HF-SF	$[Cu^{(I/II)}(dmby)_2]$	0.73	100.9	80.1	28.23

Table S10. *J-V* data for normal and HF-SF DSCs using D35:XY1b co-sensitized dye with $[Cu^{(I/II)}(dmp)_2]$ and $[Cu^{(I/II)}(dmby)_2]$ electrolytes under 500 lux WW LED illumination (P_{in} – 150.10 μW/cm^2).

DEVICE	ELECTROLYTE	V_{OC} (V)	J_{SC} (MA/CM^2)	*FF*	EFFICIENCY (%)
Normal		0.75	63.3	77.5	24.6
HF-SF	$[Cu^{(I/II)}(dmp)_2]$	0.74	67.5	78.8	26.3
Normal		0.72	69.2	78.5	25.9

HF-SF	$[Cu^{(I/II)}(dmby)_2]$	0.72	73.7	79.7	28.1

Table S11. *J-V* data for normal and HF-SF DSCs using D35:XY1b co-sensitized dye with $[Cu^{(I/II)}(dmp)_2]$ and $[Cu^{(I/II)}(dmby)_2]$ electrolytes under 200 lux WW LED illumination (P_{in} – 65.23 μW/cm^2).

DEVICE	ELECTROLYTE	V_{OC} (V)	J_{SC} (MA/CM^2)	*FF*	EFFICIENCY (%)
Normal	$[Cu^{(I/II)}(dmp)_2]$	0.70	20.67	73.2	16.4
HF-SF		0.70	24.61	72.0	19.2
Normal	$[Cu^{(I/II)}(dmby)_2]$	0.67	19.12	81.4	16.0
HF-SF		0.68	24.55	80.6	20.6

Table S12. *J-V* data for normal and HF-SF DSCs using D35:XY1b co-sensitized dye with $[Cu^{(I/II)}(dmp)_2]$ and $[Cu^{(I/II)}(dmby)_2]$ electrolytes under 100 lux WW LED illumination (P_{in} – 30.43 μW/cm^2).

DEVICE	ELECTROLYTE	V_{OC} (V)	J_{SC} (MA/CM^2)	*FF*	EFFICIENCY (%)
Normal	$[Cu^{(I/II)}(dmp)_2]$	0.67	9.56	67.0	14.3
HF-SF		0.66	10.83	66	15.9
Normal	$[Cu^{(I/II)}(dmby)_2]$	0.65	10.83	83.7	19.8
HF-SF		0.65	11.81	78.5	20.1

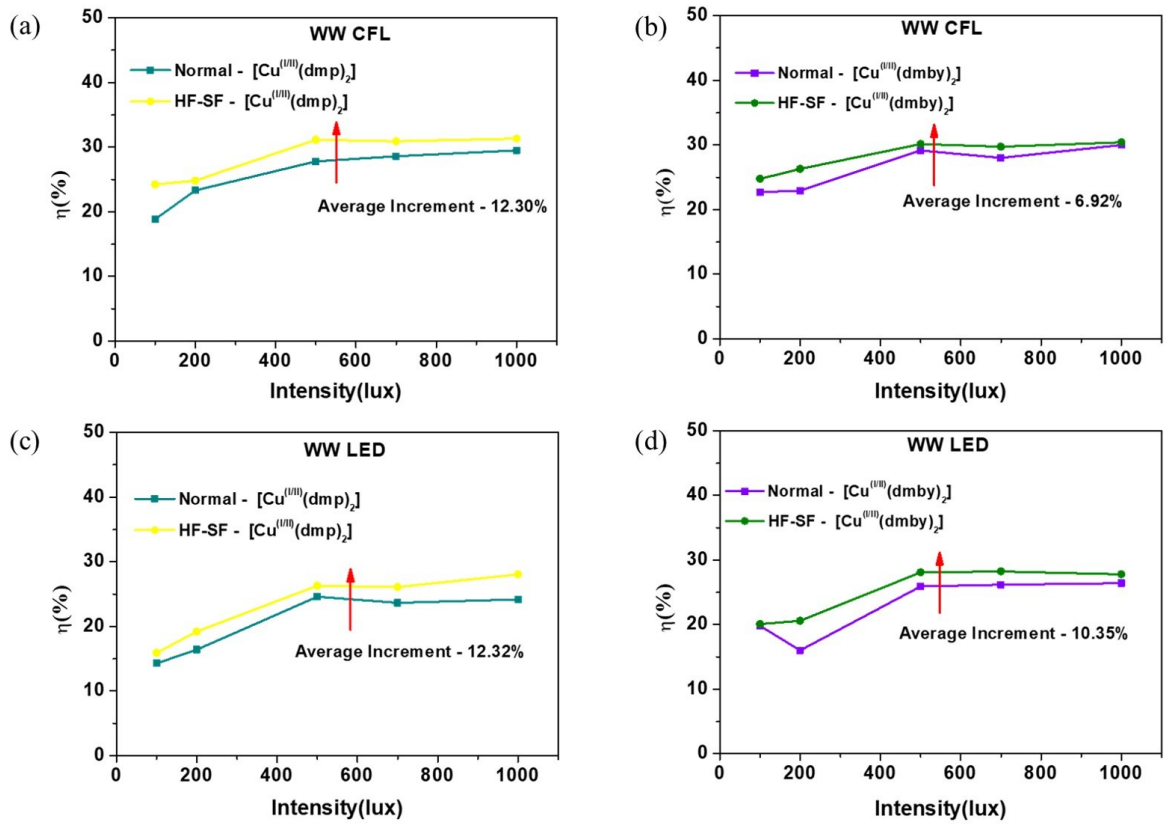

Figure S7. Variation in efficiency for normal and HF-SF DSCs under different illumination intensities (1000 – 100 lux) using WW CFL and WW LED light source employing $[Cu^{(I/II)}(dmp)_2]$ and $[Cu^{(I/II)}(dmby)_2]$ electrolytes using co-sensitized D35:XY1b dye.

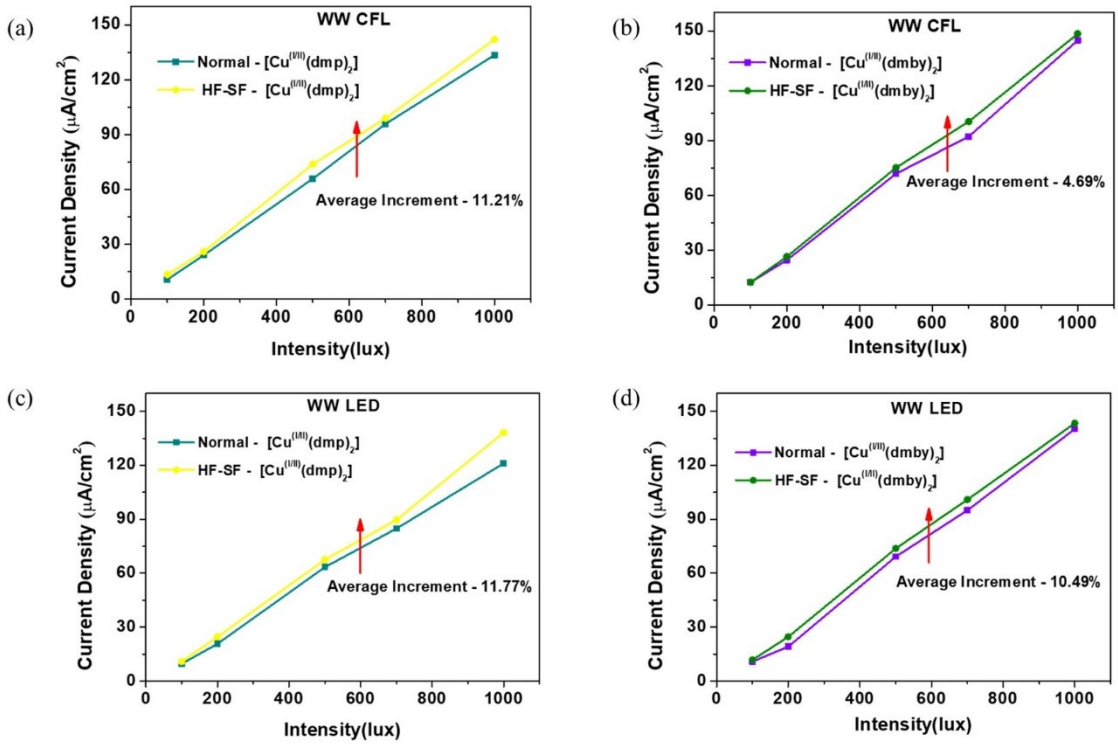

Figure S8. Variation in current density for normal and HF-SF DSCs under different illumination intensities (1000 – 100 lux) using WW CFL and WW LED light source employing $[Cu^{(I/II)}(dmp)_2]$ and $[Cu^{(I/II)}(dmby)_2]$ electrolytes using co-sensitized D35:XY1b dye.

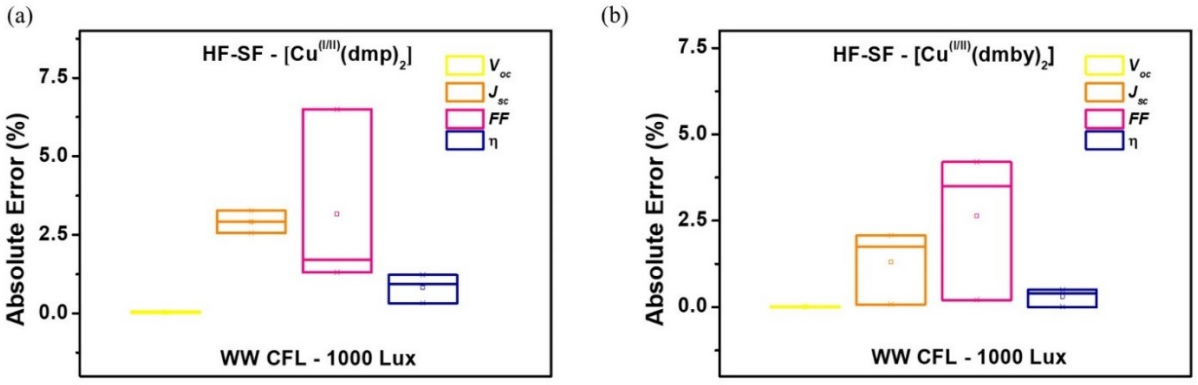

Figure S9. Absolute error plot for HF-SF DSCs employing **(a)** $[Cu^{(I/II)}(dmp)_2]$ and **(b)** $[Cu^{(I/II)}(dmby)_2]$ electrolytes.

Table S13. *J-V* data for large area normal and HF-SF DSCs using D35:XY1b co-sensitized dye and $[Cu^{(I/II)}(dmp)_2]$ electrolyte under 1000 lux WW CFL illumination (P_{in} – 283.41 μW/cm^2).

DEVICE	V_{OC} (V)	J_{SC} (MA/CM^2)	I_{SC} (MA)	POWER (MW)	*FF*	EFFICIENCY (%)
Normal	0.72	124.70	240.17	137.7	79.2	25.34
HF-SF	0.75	144.37	277.19	159.5	76.5	29.35

Table S14. *J-V* data for large area normal and HF-SF DSCs using D35:XY1b co-sensitized dye and $[Cu^{(I/II)}(dmp)_2]$ electrolyte under 700 lux WW CFL illumination (P_{in} – 195.45 μW/cm^2).

DEVICE	V_{OC} (V)	J_{SC} (MA/CM^2)	I_{SC} (MA)	POWER (MW)	*FF*	EFFICIENCY (%)
Normal	0.72	85.1	163.5	90.98	77.3	24.30
HF-SF	0.74	100.7	193.4	108.4	75.3	28.96

Table S15. *J-V* data for large area normal and HF-SF DSCs using D35:XY1b co-sensitized dye and $[Cu^{(I/II)}(dmp)_2]$ electrolyte under 500 lux WW CFL illumination (P_{in} – 143.05 μW/cm^2).

DEVICE	V_{OC} (V)	J_{SC} (MA/CM^2)	I_{SC} (MA)	POWER (MW)	*FF*	EFFICIENCY (%)
Normal	0.71	64.77	124.4	70.0	79	25.5
HF-SF	0.74	71.9	138.1	77.7	76.5	28.3

Table S16. *J-V* data for large area normal and HF-SF DSCs using D35:XY1b co-sensitized dye and $[Cu^{(I/II)}(dmp)_2]$ electrolyte under 200 lux WW CFL illumination (P_{in} – 59.11 μW/cm^2).

DEVICE	V_{OC} (V)	J_{SC} (MA/CM^2)	I_{SC} (MA)	POWER (MW)	*FF*	EFFICIENCY (%)
Normal	0.67	22.3	42.8	21.1	73.1	18.64
HF-SF	0.70	27.56	52.9	26.4	70.5	23.29

Table S17. *J-V* data for large area normal and HF-SF DSCs using D35:XY1b co-sensitized dye and [$Cu^{(I/II)}(dmp)_2$] electrolyte under 100 lux WW CFL illumination (P_{in} – 28.47 μW/cm²).

DEVICE	V_{OC} (V)	J_{SC} (MA/CM²)	I_{SC} (MA)	POWER (MW)	*FF*	EFFICIENCY (%)
Normal	0.66	12.9	24.8	11.75	71.9	21.87
HF-SF	0.68	15.2	29.25	14.15	70.6	26.32

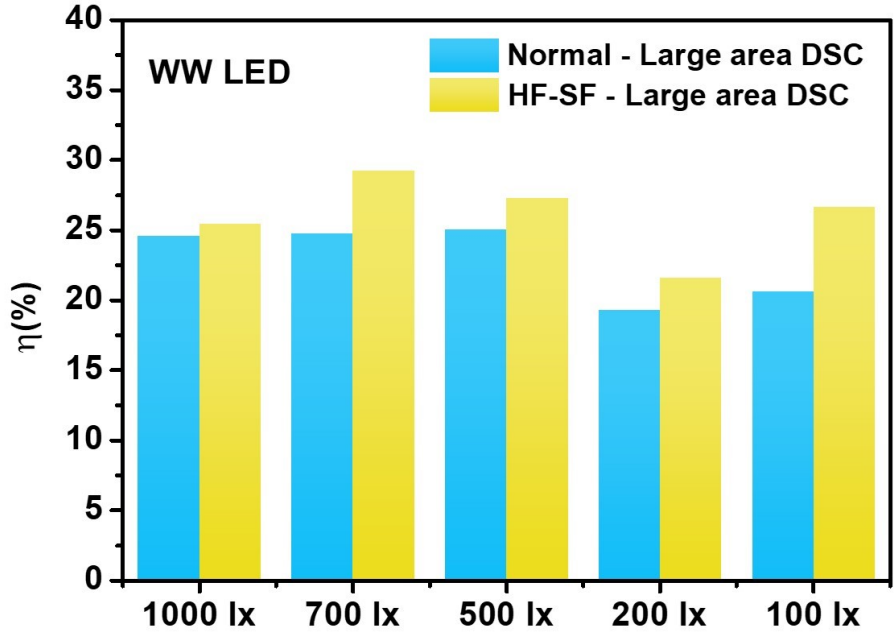

Figure S10. Efficiency as a function of illumination intensity for normal and HF-SF large area DSCs under WW LED illumination (1000 – 100 lux) employing [$Cu^{(I/II)}(dmp)_2$] electrolyte using co-sensitized D35:XY1b dyes.

Table S18. *J-V* data for normal and HF-SF large area DSCs using D35:XY1b co-sensitized dye with [$Cu^{(I/II)}(dmp)_2$] electrolyte under 1000 lux WW LED illumination (P_{in} -303.16 μW/cm²).

DEVICE	V_{OC} (V)	J_{SC} (MA/CM²)	I_{SC} (MA)	POWER (MW)	*FF*	EFFICIENCY (%)
Normal	0.73	137.52	264.04	142.82	73.7	24.55
HF-SF	0.73	144.99	277.86	147.99	72.1	25.44

Table S19. *J-V* data for normal and HF-SF large area DSCs using D35:XY1b co-sensitized dye with $[Cu^{(I/II)}(dmp)_2]$ electrolyte under 700 lux WW LED illumination (P_{in} -208.94 μW/cm^2).

DEVICE	V_{OC} (V)	J_{SC} (MA/CM^2)	I_{SC} (MA)	POWER (MW)	*FF*	EFFICIENCY (%)
Normal	0.73	90.7	174.21	99.31	78.4	24.75
HF-SF	0.73	111.6	214.27	117.24	74.6	29.22

Table S20. *J-V* data for normal and HF-SF large area DSCs using D35:XY1b co-sensitized dye with $[Cu^{(I/II)}(dmp)_2]$ electrolyte under 500 lux WW LED illumination (P_{in} -150.10 μW/cm^2).

DEVICE	V_{OC} (V)	J_{SC} (MA/CM^2)	I_{SC} (MA)	POWER (MW)	*FF*	EFFICIENCY (%)
Normal	0.72	69.9	134.23	74.90	77.6	25.01
HF-SF	0.72	76.08	146.08	78.59	74.2	27.29

Table S21. *J-V* data for normal and HF-SF large area DSCs using D35:XY1b co-sensitized dye with $[Cu^{(I/II)}(dmp)_2]$ electrolyte under 200 lux WW LED illumination (P_{in} - 65.23 μW/cm^2).

DEVICE	V_{OC} (V)	J_{SC} (MA/CM^2)	I_{SC} (MA)	POWER (MW)	*FF*	EFFICIENCY (%)
Normal	0.71	24.06	46.19	24.01	73.2	19.29
HF-SF	0.69	25.42	48.81	26.74	79.4	21.59

Table S22. *J-V* data for normal and HF-SF large area DSCs using D35:XY1b co-sensitized dye with $[Cu^{(I/II)}(dmp)_2]$ electrolyte under 100 lux WW LED illumination (P_{in} - 30.43 μW/cm^2).

DEVICE	V_{OC} (V)	J_{SC} (MA/CM^2)	I_{SC} (MA)	POWER (MW)	*FF*	EFFICIENCY (%)
Normal	0.66	12.89	24.76	11.88	72.2	20.63
HF-SF	0.68	15.5	29.86	15.34	75.4	26.64

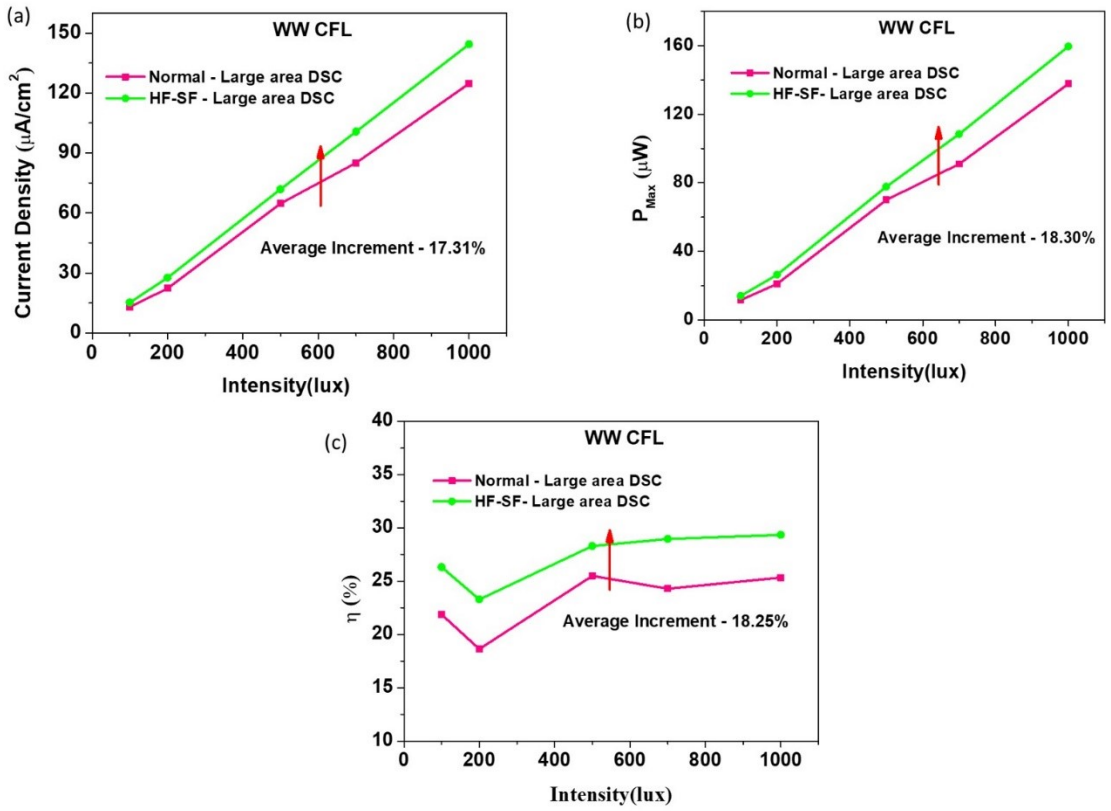

Figure S11. Variation in **(a)** current density, **(b)** power output (P_{max}), and **(c)** efficiency (η) as a function of illumination intensity (1000 – 100 lux) using WW CFL light source for normal and HF-SF large area DSCs using co-sensitized D35:XY1b dye and $[Cu^{(I/II)}(dmp)_2]$ electrolyte.

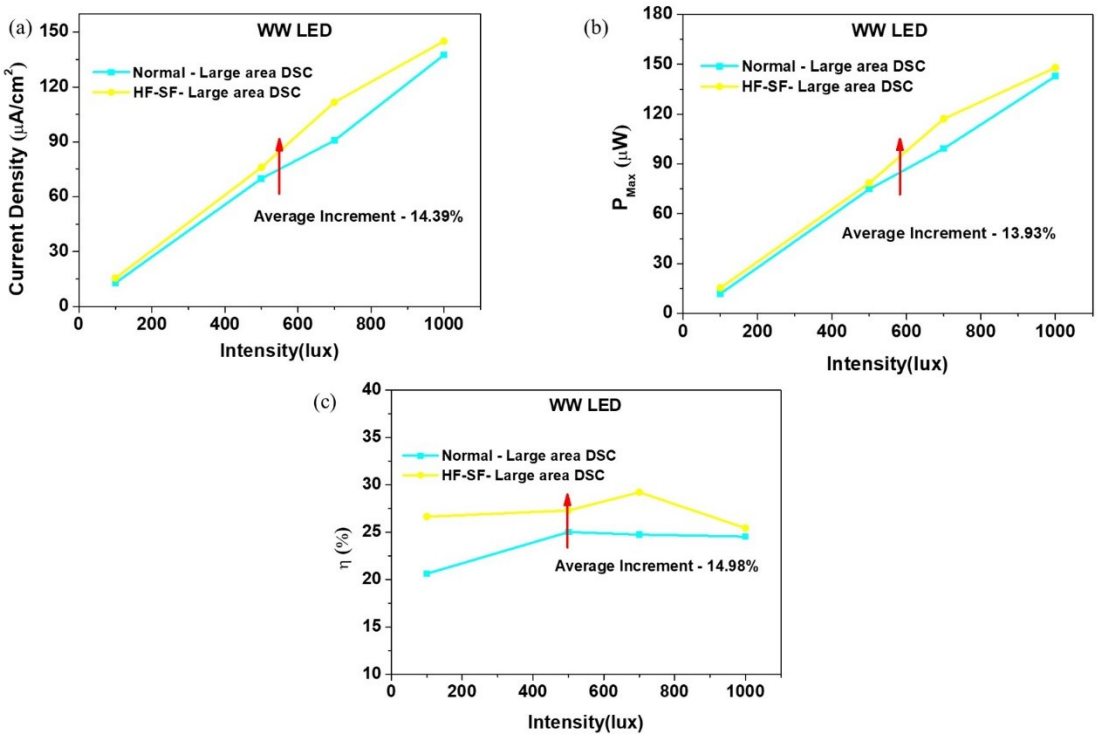

Figure S12. Variation in **(a)** current density, **(b)** power output (P_{max}), and **(c)** efficiency (η) as a function of illumination intensity (1000 – 100 lux) using WW LED light source for normal and HF-SF large area DSCs using co-sensitized D35:XY1b dye and $[Cu^{(I/II)}(dmp)_2]$ electrolyte.

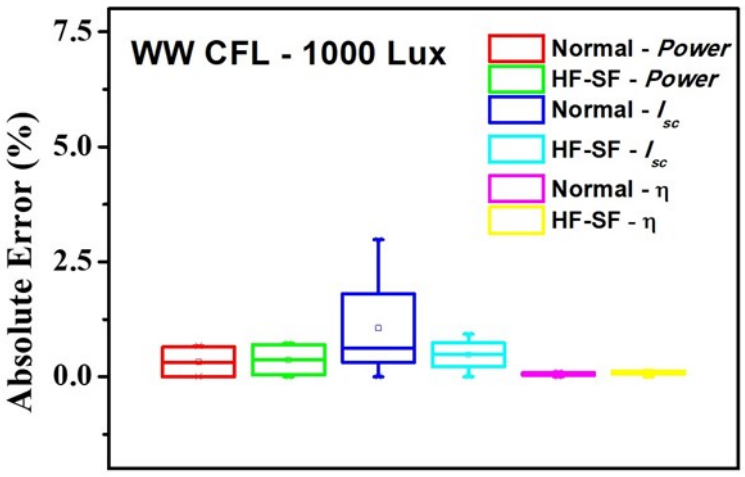

Figure S13. Absolute error plot for large area normal and HF-SF DSCs under WW CFL 1000 lux illumination employing $[Cu^{(I/II)}(dmp)_2]$ electrolyte along with co-sensitized D35:XY1b dyes.

Table S23. Comparison between Normal and HF-SF device architecture.

Device	Active area	FTO Area (Photoanode)	Active area/FTO	Electrolyte required/device
Normal device	1.92 cm^2 (2.4cm x 0.8cm)	3.6 cm^2 (3cm x 1.2cm)	53.3%	16-20 µL
HF-SF device	1.92 cm^2 (2.4cm x 0.8cm)	2.00 cm^2 (2.5cm x 0.8cm)	96.0%	8-10 µL

Table S24. Average increment in active area: FTO area for HF-SF device compared to normal device, average decrease in FTO cost and electrolyte requirement for HF-SF device compared to normal device.

Average increment in active area:FTO ratio for HF-SF device	**80%**
Average reduction in FTO cost for HF-SF device	**40%**
Average reduction in electrolyte required per device	**50%**

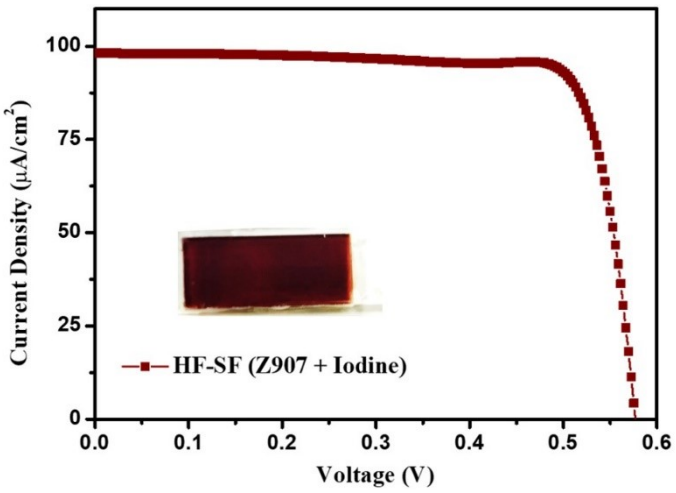

Figure S14. *J-V* plot for large area HF-SF DSCs using Z907 dye and commercial HSE iodine electrolyte.

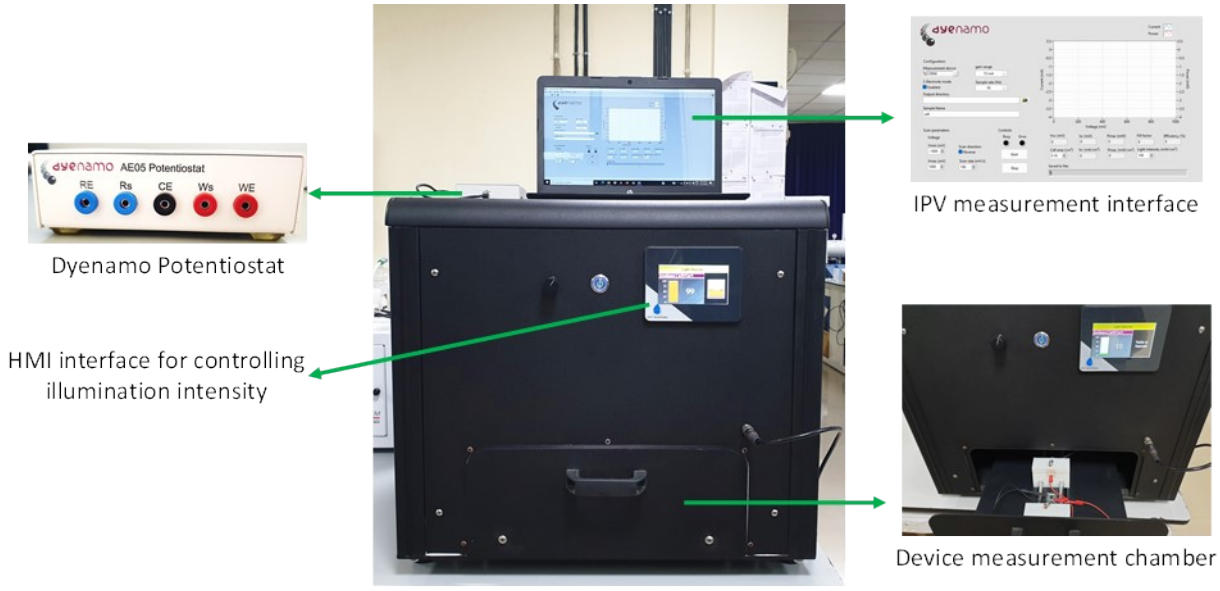

Figure S15. Custom designed Indoor light soaker used to perform accelerated stability measurements.

Table S25. J-V data for large area HF-SF DSCs fabricated using Z907 dye and iodine HSE electrolyte.

Device	V_{oc} (V)	J_{sc} (μA/cm^2)	I_{sc} (μA)	Power (μW)	*FF*	Efficiency (%)
HF-SF Device (Z907 + Iodine)	0.58	95.17	188.43	89.4	82.1	15.95

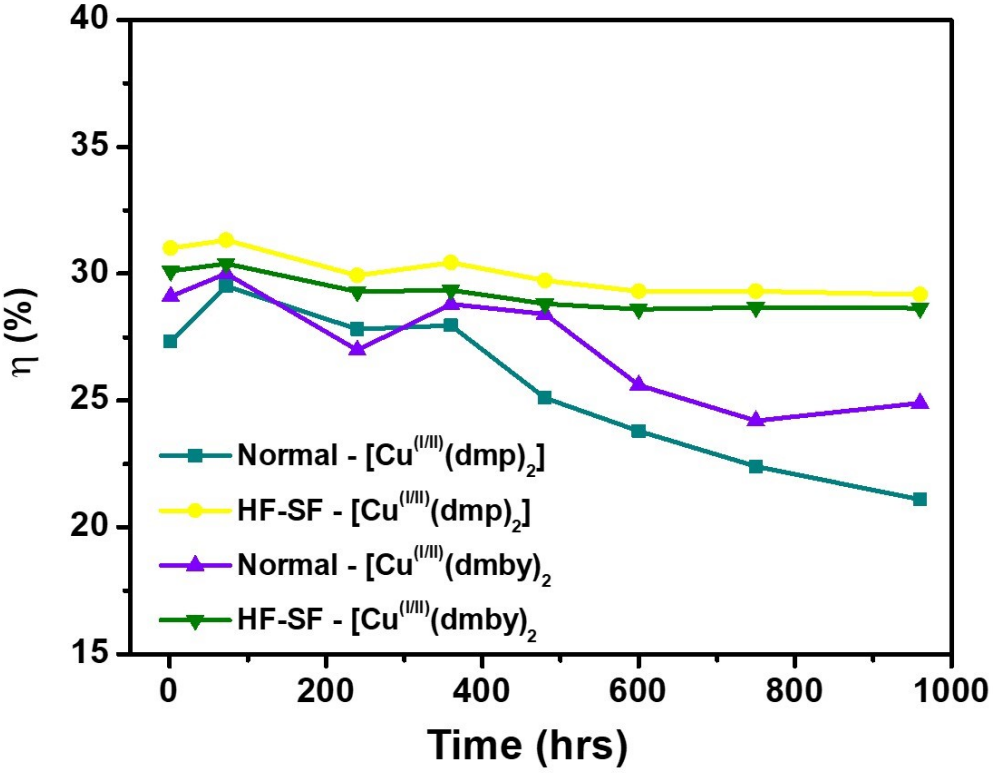

Figure S16. 1000 hours stability data for HF-SF devices employing $[Cu^{(I/II)}(dmp)_2]$ and $[Cu^{(I/II)}(dmby)_2]$ electrolytes using co-sensitized D35:XY1b dyes under continuous light soaking using a custom made LED light soaker under 80% R.H.

Table S26. *J-V* data for HF-SF modules connected in series under 1000 lux WW CFL illumination employing $[Cu^{(I/II)}(dmp)_2]$ electrolyte and co-sensitized D35:XY1b dyes.

Device	V_{OC} (V)	I_{SC} (µA)	FF	Power (µW)
HF-SF DSC modules connected in series	1.39	546.02	64.0	485.9

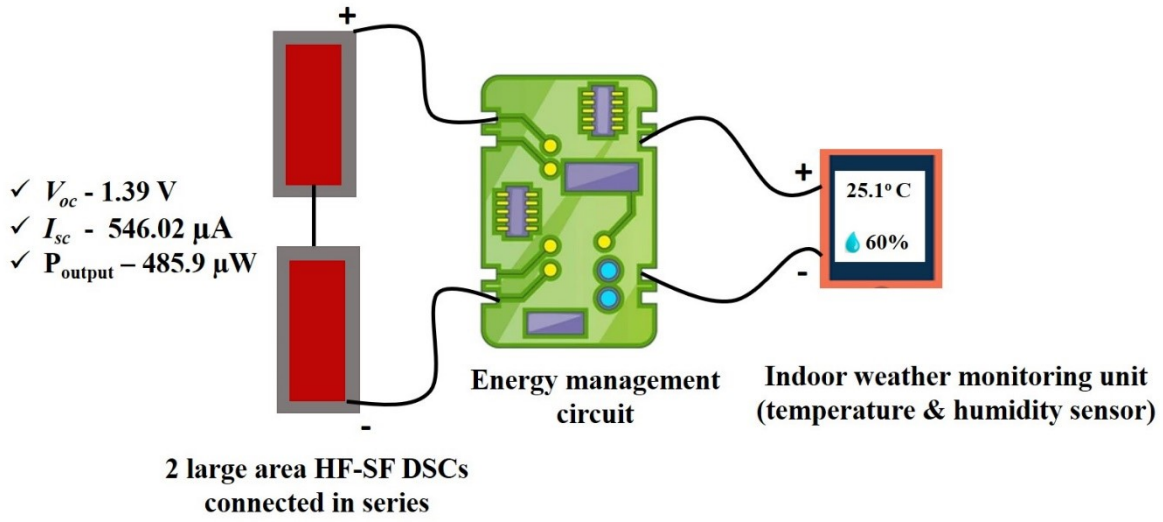

Scheme S2. Schematic representation of the energy management circuit and its integration with the HF-SF DSCs and display unit.

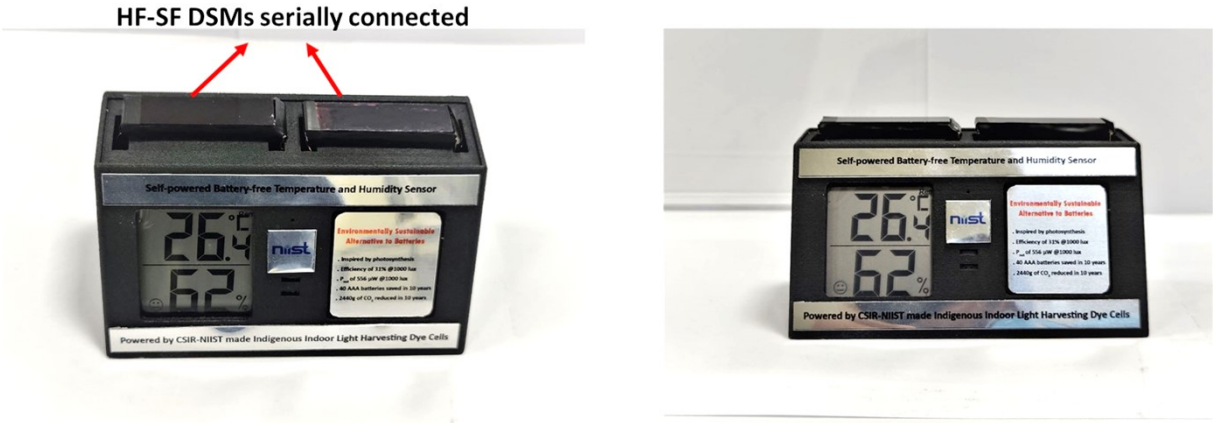

Figure S17. Indoor weather monitoring unit (temperature and humidity sensor) powered by serially interconnected HF-SF DSMs using co-sensitized D35:XY1b dyes and $[Cu^{(I/II)}(dmp)_2]$ electrolyte.

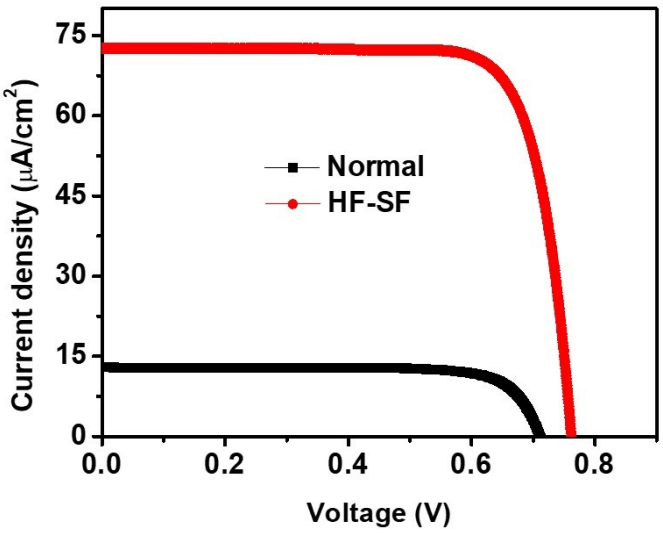

Figure S18. *J-V* graph for normal and HF-SF DSCs under 1000 lux WW CFL back-side illumination using $[Cu^{(I/II)}(dmp)_2]$ electrolyte and co-sensitized D35:XY1b dyes.

Table S27. *J-V* data for normal and HF-SF DSCs under 1000 lux WW CFL back-side illumination using $[Cu^{(I/II)}(dmp)_2]$ electrolyte and co-sensitized D35:XY1b dyes.

Device	V_{OC} (V)	J_{SC} (μA/cm²)	FF	Efficiency (%)
Normal	0.71	13.1	76.6	2.51
HF-SF	0.76	72.6	79.0	15.45

References

1 J. Velore, S. Chandra Pradhan, T. W. Hamann, A. Hagfeldt, K. N. N. Unni and S. Soman, *ACS Appl. Energy Mater.*, 2022, **5**, 2647–2654.

2 S. C. Pradhan, J. Velore, A. Hagfeldt and S. Soman, *J. Mater. Chem. C*, 2022, **10**, 3929–3936.

3 S. C. Pradhan, A. Hagfeldt and S. Soman, *J. Mater. Chem. A*, 2018, **6**, 22204–22214.

4 R. Haridas, J. Velore, S. C. Pradhan, A. Vindhyasarumi, K. Yoosaf, S. Soman, K. N. N. Unni and A. Ajayaghosh, *Mater. Adv.*, 2021, **2**, 7773–7787.